# EXPERIMENTAL AND NUMERICAL EVALUATION OF CRASH AND IMPACT LOADED TEXTILE REINFORCED THERMOPLASTIC COMPONENTS

W. A. Hufenbach[1], A. Langkamp[1], A. Hornig[1*], H. Böhm[1], T. Weber[1], M. Berthel[1]

[1] *Institute of Lightweight Engineering and Polymer Technology, Technische Universität Dresden, Holbeinstraße 3, 01307 Dresden, Germany*
** Andreas.Hornig@TU-Dresden.de (corresponding author)*

**Keywords:** textile composites, crash and impact, numerical analysis, strain rate dependency.

**Abstract**
*The crash and impact behaviour of textile reinforced thermoplastics is investigated. Firstly, a strain rate dependent parameter identification strategy for a multi-layered flat bed weft-knitted fabric (MKF) and a woven fabric (Twintex®) is discussed. In addition to that, in total 29 crash and impact verification test cases were performed. A phenomenological 3D material model based on the Cuntze failure criteria, accounting for strain rate dependency and damage evolution is presented. In Abaqus/Explicit a user defined material model (VUMAT) is used to apply the elaborated material model within finite element (FE) studies of the crash and impact experiments. Exemplary numerical and experimental results are presented and compared.*

## 1 Introduction

With short cycle times for a highly productive manufacturing process and excellent specific mechanical properties, textile reinforced thermoplastic composites are predestined for the development and design of material and energy efficient lightweight structures. Especially due to their high energy absorption capacity, this material group is increasingly considered for applications in the field of crash and impact resistant design.

However, with regard to the complex loading conditions resulting from crash and impact configurations there is still a lack of well founded knowledge especially in the field of the damage and failure behaviour of composites with textile reinforcement. Besides non-linear material characteristics, the through-thickness properties and the related delamination behaviour play a key role in that respect. Furthermore, the mechanical behaviour of materials strongly depends on the velocity of the load application. The consideration of the effects of a rapid increase of the strain rate on the orthotropic material characteristics is essential in order to achieve a reliable design strategy.

In the presented investigations two glass/polypropylene (GF/PP) textile composite configurations are characterized with regard to in-plane as well as trough thickness material properties [1],[2]. The determined characteristics are used within a phenomenological 3D damage model [3][4] based on the failure mode concept of Cuntze [5]. With the scope on crash and impact loading conditions, strain rate dependency is taken into account by a Johnson-Cook approach [6]. The results of the presented experimental crash and impact

investigations on structural level are used for numerical studies within in the FE-software Abaqus/Explicit. For that the proposed material model was implemented using a VUMAT. For model validation in terms of the structural deformation and failure behaviour the experimental and numerical results are compared.

## 2 Parameter identification and material modeling

*2.1 Material configurations and identification of strain rate dependent properties*

For the investigations two glass/polypropylene (GF/PP) hybrid yarn based textile composite configurations have been considered, namely a multi-layered flat bed weft-knitted fabric (MKF) and a woven fabric (Twintex®). The MKF with a fibre volume fraction of 48 % is uniquely produced by the Technische Universität Dresden, Institute of Textile Machinery and High Performance Material Technology (ITM) and offers excellent draping and crash properties [7]. Twintex® TPP 60 745 is supplied by Saint-Gobain Vetrotex and is a 2/2 twill weave with a fibre volume fraction of 35 %.

It is well known that the mechanical behaviour of materials strongly depends on the velocity of the load application. Under consideration of the direction dependency and with the scope on highly dynamic loading conditions and the related material modelling these effects are to be taken into account, especially for the used combination of glass fibres and polypropylene matrix. The experimental determination of strain rate dependent material properties like elastic moduli, strength and failure strains therefore demands adapted testing methods.

A servo hydraulic high velocity test system INSTRON VHS 160/20 has been used for the determination of in-plane material characteristics with deformation velocities of up to 20 m/s and a maximum force of 160 kN. Adaptations of the test equipment allowed highly dynamic tensile, compression and shear tests (Figure1). A high speed camera system in combination with a system for non-contact optical 3D deformation analysis (ARAMIS) was used to evaluate the dislocation and distortion fields and to calculate the corresponding strain field and strain rate.

The specimens are exposed to the testing load not until the designated test velocity has been reached and therefore a constant strain rate is achieved over the test duration. Exemplary results and more detailed information can be found in [8]-[10]. The shear deformation behavior was characterized using a lightweight Iosipescu-setup. Initial results and further details are given in [11]. Amongst others, more recent investigations of the highly non-linear shear behavior were used for the material model calibration, whereas selected ones are presented in Figure 2.

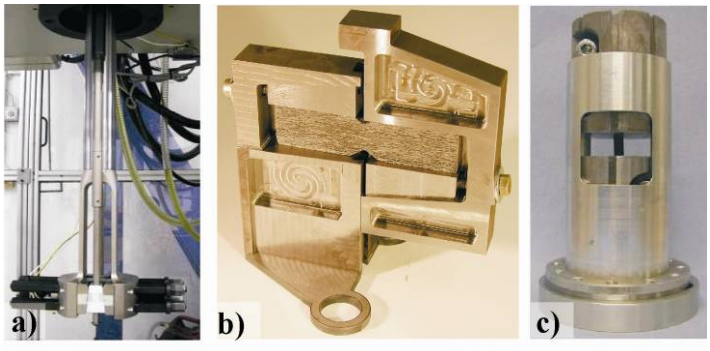


**Figure 1.** Devices for the servo hydraulic high velocity system: a) tension, b) shear and c) compression unit. [8]

With the focus on crash and impact loading conditions, the induced complex 3D stress and deformation states demand the determination of through-thickness properties. In this respect, extensive investigations were performed. An overview of these efforts is given in [12].

The investigations showed that the commonly used Split Hopkinson Bar method does not lead to reliable results. The coarse textile architecture demands adapted specimen dimensions and designs. One approach using L-shaped beam specimens is explained in detail in [2].

*2.2 Material model*

The used phenomenological material model is based on a continuum mechanical approach to predict direction dependent and mode related failure based on Cuntze [5]. An accumulative and mode related damage evolution assures a successive stiffness degradation for each orthotropic textile layer [3],[4]. It is based on the assumption of linear-elastic material behaviour up to an initial damage threshold characterized by the damage strength $R_{di\ t/c}$ for each direction, with *t* denoting tension and *c* compression. The damage evolution effects induce stress-strain non-linearities up to final failure $R_{it/c}$. Additionally, strain rate dependency is considered by a scaling function for the strengths and stiffness parameters.
Onset of damage is described by the following criterion:

$$H^n = \left(\frac{\sigma_1^+}{R_{d1t}}\right)^n + \left(\frac{\sigma_1^-}{R_{d1c}}\right)^n + \left(\frac{\sigma_2^+}{R_{d2t}}\right)^n + \left(\frac{\sigma_2^-}{R_{d2c}}\right)^n + \left(\frac{\sigma_3^+}{R_{d3t}}\right)^n + \left(\frac{\sigma_3^-}{R_{d3c}}\right)^n + \left(\frac{\tau_{12}}{R_{d12}}\right)^n + \left(\frac{\tau_{31}}{R_{d31}}\right)^n + \left(\frac{\tau_{23}}{R_{d23}}\right)^n = 1 \qquad (1)$$

with *n* defining the failure envelope. After initiation, the damage $D_i$ is taken into account by stiffness degradation through

$$\tilde{E}_i = E_i(1 - D_i) \qquad \text{with} \qquad D_i = 0 \ldots 1 \quad , \qquad (2)$$

where the attenuated elastic properties $\tilde{E}_i$ are calculated based on the elastic properties $E_i^T = E_1, E_2, E_3, G_{12}, G_{23}, G_{31}$. Damage evolution is modelled by

$$D_i = \left(q_{ij}\Phi_j^n\right)^{\frac{1}{n}} \qquad \text{and} \qquad q_{ij} = \begin{bmatrix} 1 & 1 & 0 & 0 & 0 & 0 & 0 & 0 & 0 \\ 0 & 0 & 1 & 1 & 0 & 0 & 0 & 0 & 0 \\ 0 & 0 & 0 & 0 & 1 & 1 & 0 & 0 & 0 \\ 0 & 0 & 0 & 0 & 0 & 0 & 1 & 0 & 0 \\ 0 & 0 & 0 & 0 & 0 & 0 & 0 & 1 & 0 \\ 0 & 0 & 0 & 0 & 0 & 0 & 0 & 0 & 1 \end{bmatrix} . \qquad (3)$$

The coupling matrix $q_{ij}$ considers the coupling effects in the mode related damage evolution for each failure mode *j* (1…9) and the elastic properties *i* (1,2,3,12,23,31). The evolution law

$$\Phi_j = \tanh\left(\beta_j\left(r_j - r_j^0\right)^{\kappa_j}\right) \qquad (4)$$

considers the mode related efforts at the current stage $r_j$ and at initial failure $r_i^0$ for the following nine modes

$$r_1 = \frac{\sigma_1^+(1-D_1)}{R_{d1t}} \quad , \qquad r_2 = \frac{\sigma_1^-(1-D_1)}{R_{d1c}} \quad , \qquad r_3 = \frac{\sigma_2^+(1-D_2)}{R_{d2t}} \quad ,$$
$$r_4 = \frac{\sigma_2^-(1-D_2)}{R_{d2c}} \quad , \qquad r_5 = \frac{\sigma_3^+(1-D_3)}{R_{d3t}} \quad , \qquad r_6 = \frac{\sigma_3^-(1-D_3)}{R_{d3c}} \quad , \qquad (5)$$

$$r_7 = \frac{|\tau_{12}|(1-D_4)}{R_{d12}} \quad , \qquad r_8 = \frac{|\tau_{23}|(1-D_5)}{R_{d23}} \quad , \qquad r_9 = \frac{|\tau_{31}|(1-D_6)}{R_{d31}} \quad ,$$

as well as the parameter $\beta_j$, which can be interpreted as the driving damage growth parameter and the additional parameter $\kappa_j$, which is used to model a smooth or non-smooth transition from the elastic to the damage stage. Strain rate dependency is related to the elastic and strength parameters and was found to be accurately described by the Johnson-Cook [6] based equation

$$E_i^0(\dot{\varepsilon}_i) = E_i^{0,\mathrm{ref}}\left[1 + a_i \ln\left(\frac{\dot{\varepsilon}_i}{\dot{\varepsilon}_i^{\mathrm{ref}}}\right)\right] \qquad \text{and} \qquad R_i^0(\dot{\varepsilon}_i) = R_i^{0,\mathrm{ref}}\left[1 + c_i \ln\left(\frac{\dot{\varepsilon}_i}{\dot{\varepsilon}_i^{\mathrm{ref}}}\right)\right] \quad . \tag{6}$$

Here, $E_i^0$ and $R_i^0$ represent the initial, undamaged stiffness and strength parameters at the current strain rate $\dot{\varepsilon}_i$. With the reference values $E_i^{0,ref}$ and $R_i^{0,ref}$ at a reference strain rate $\dot{\varepsilon}_i^{ref}$ and the material constants $a_i$ and $c_i$, an adapted slope for higher strain rate values can be achieved. Final failure, resulting in element erosion, is calculated by

$$F^m = \left(\frac{\sigma_1^+}{R_{1t}}\right)^m + \left(\frac{\sigma_1^-}{R_{1c}}\right)^m + \left(\frac{\sigma_2^+}{R_{2t}}\right)^m + \left(\frac{\sigma_2^-}{R_{2c}}\right)^m + \left(\frac{\sigma_3^+}{R_{3t}}\right)^m + \left(\frac{\sigma_3^-}{R_{3c}}\right)^m + \left(\frac{\tau_{12}}{R_{12}}\right)^m + \left(\frac{\tau_{31}}{R_{31}}\right)^m + \left(\frac{\tau_{23}}{R_{32}}\right)^m = 1 \quad . \tag{7}$$

The presented model has been implemented in the FE software Abaqus/Explicit through a VUMAT. It was used for the numerical studies based on the determined material characteristics. Exemplary model predictions vs. experimental values are displayed in Figure 2. It illustrates the capability of the model to predict the highly non-linear shear behaviour and the pronounced strain rate dependency.

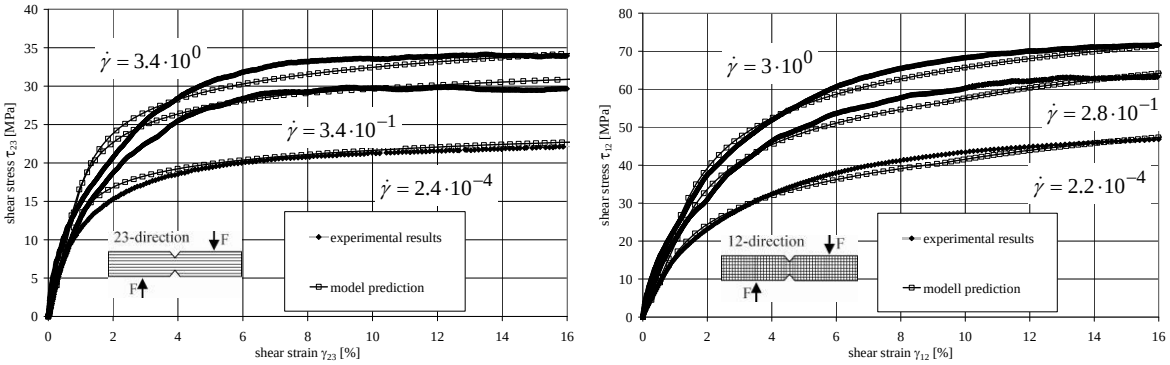


**Figure 2.** Strain rate dependent through-thickness (left) and in-plane shear behaviour (right): Comparison of experimental results and numerical model predictions

## 3 Crash and impact testing

### *3.1 Impact experiments*

Besides experimental work on material characterization on coupon testing level (Sec. 2.1) an experimental program was performed to investigate the highly dynamic material response on structural level with an emphasis on crash and impact loading conditions. In case of the impact testing, plane and curved specimens were tested at velocities of up to 115 m/s. The focus in this paper lies on lies on the latter ones, where the behaviour of MKF and Twintex® was compared. The test setup for 24 impact experiments is presented in Fig. 6. The specimens

(150 x 220 mm, 4, 8, 16 layers) are impacted by a polyamide-epoxy projectile with a weight of 100 g and a diameter of 40 mm. The high speed camera system in combination with ARAMIS for non-contact optical 3D deformation analysis was used to determine the deflections, whereas the post experimental failure and damage analysis was based on optical, ultrasonic and CT evaluations (Figure 4).

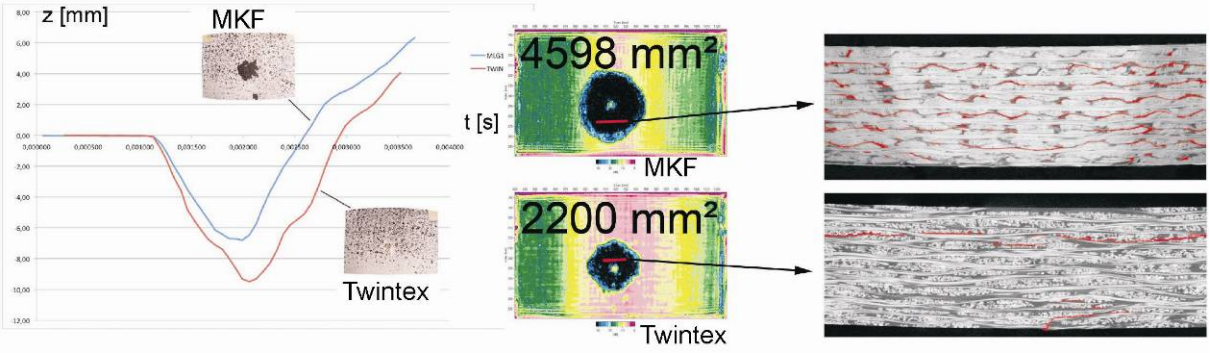


**Figure 4.** Comparison of impacted MKF and Twintex curved specimen (thickness 8mm): deflection during impact (left), delamination areas based on C-scans (middle) and corresponding CT scans with indicated delaminations (right)

As a result of the experiments, the critical impact velocity (fibre ruptures) for both 8 mm thick material configurations was identified at $v = 43$ m/s (~95 J). The maximal deflection for Twintex results in 9.5 mm and for MKF in 6.8 mm. In general, the MKF material exhibits lower deflections and therefore a higher bending stiffness due to the higher glass fibre volume fraction. In contrast is shows less delamination resistance than the Twintex material (Figure 4). This correlates well with the CT results, which indicate that the amount of delaminations over the specimen thickness is significantly lower than in the MKF specimens.

*3.2 Crash experiments*

The crash experiments were performed using a drop tower setup with weights of up to 390 kg at different levels of structural complexity. Besides the axial compression behaviour of plane and curved spacer components, bonded components under 0° and 45° loading were in focus here. Additionally, a front section structure of a generic technology demonstrator was tested. An overview of the conducted testing program is given in Table 1.

| component | mass [kg] | drop height [m] | energy [J] |
|---|---|---|---|
| plane | 365 | 1 | 3581 |
| curved | 365 | 1 | 3581 |
| bonded 0° | 390 | 1.9 | 7154 |
| bonded 45° | 390 | 1.9 | 7158 |
| front section | - | 1 | - |

**Table 1.** Overview of the crash test experiments with spacer components

The plane (210 x 260 x 36 mm, cell connector: 2mm, Surface layer 3mm) and curved (230 x 210 x 30 mm, material thickness 1.5 mm) stitched spacer preforms were supplied by the ITM and have been manufactured within a hot pressing process. These structures were tested under axial compression. Based on a plasma surface treatment, an epoxy-adhesive (DP490 3M) was used to manufacture the bonded components (260 x 242 x 84 mm), followed by a conditioning process. An overview of the tested structures and experimental setups is given in Figure 5. In addition to the axial crushing setup, the bonded components were also tested under 45°. The front section structure (approx. 1150 x 600 x 720 mm) has been dropped

axially (Figure 8) in contrast to the other crash experiments, where the specimens were subjected to a falling mass. The deformation behaviour during the tests was analysed by the high velocity optical 3D deformation analysis. The results (Figure 6) were used for the numerical analysis and model verification.

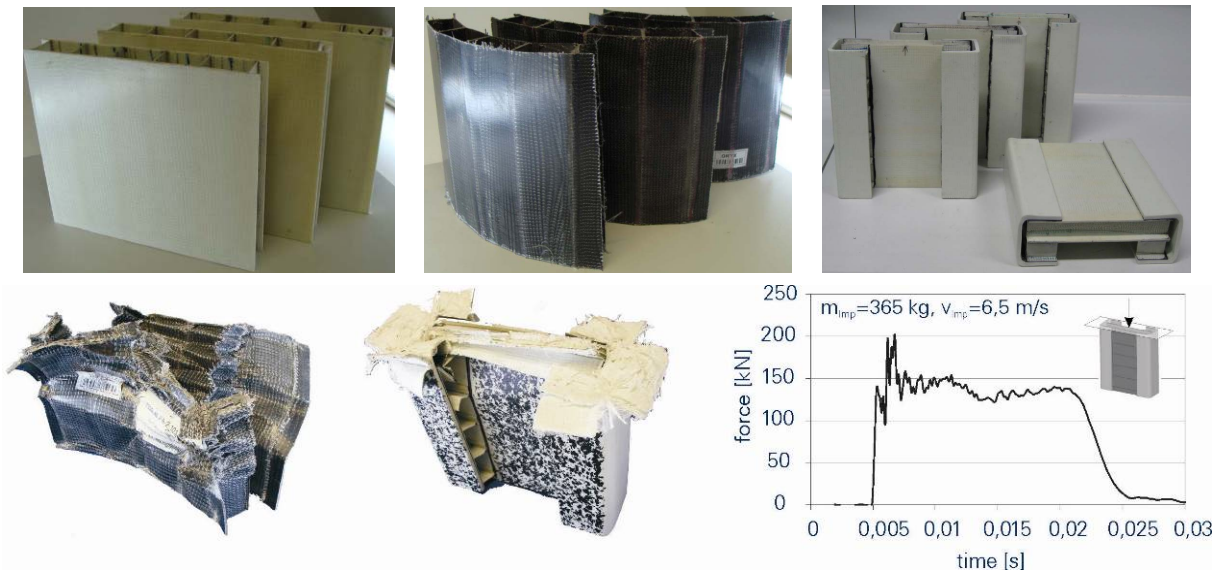


**Figure 5.** Plane (top left) curved (top middle), bonded (top right) structural components based on spacer preforms and selected results of the axial crushing experiments of curved and bonded spacer structures (bottom)

## 4 Correlation of numerical and experimental results

The discussed crash and impact loading cases (Sec. 3) have been numerically analysed using the FE software Abaqus/Explicit. For that purpose, the presented material model (Sec. 2) was implemented using a user-defined material model (VUMAT).

A special focus regarding the impact experiments is set on the occurring deformations and through-thickness failure behaviour. As displayed in Figure 6 the strain rate dependent deflection as well as damage and failure initiation is represented well by the material model within the numerical calculations. With delamination initiation and subsequent delamination propagation, the results start to divagate. This effect may be explained by elements erosion mechanisms, which prevent a delamination propagation, and clearly indicates that a characterisation of highly dynamic delamination propagation mechanisms as well as related modelling methods need to be addressed in further investigations. The plots of the delamination relevant damage mode in 23-direction confirms this trend, where the comparison to the c-scan of the impacted specimen shows an obvious under estimation (Figure 6).

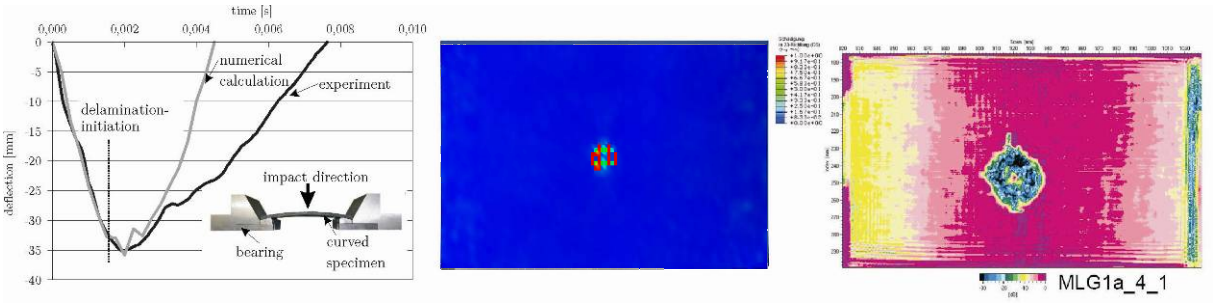


**Figure 6.** Comparison of numerical and experimental deflection curves during the impact (left), numerical prediction of the damage mode in 23-direction (middle) and c-scan of impacted specimen (right)

Deformation and failure results of the crash experiments and the comparison to the numerical simulations are displayed in Figure 7. The numerical predictions correlate well in terms of deformation patterns and failure location and timing. The dominating failure mode during the axial crushing of plane and curved spacer structures is fibre failure. In contrast, large material deformations due to through-thickness failure dominate the crashing behaviour in the bonded 0° case (see also the deformed post impact structure figure 5, bottom). A much higher meshing resolution in comparison to the impact test cases promotes the representation of a pronounced layer splitting and delamination process. Also, the structural debonding, which was modelled using cohesive elements, in the bonded 45° test case is represented well.

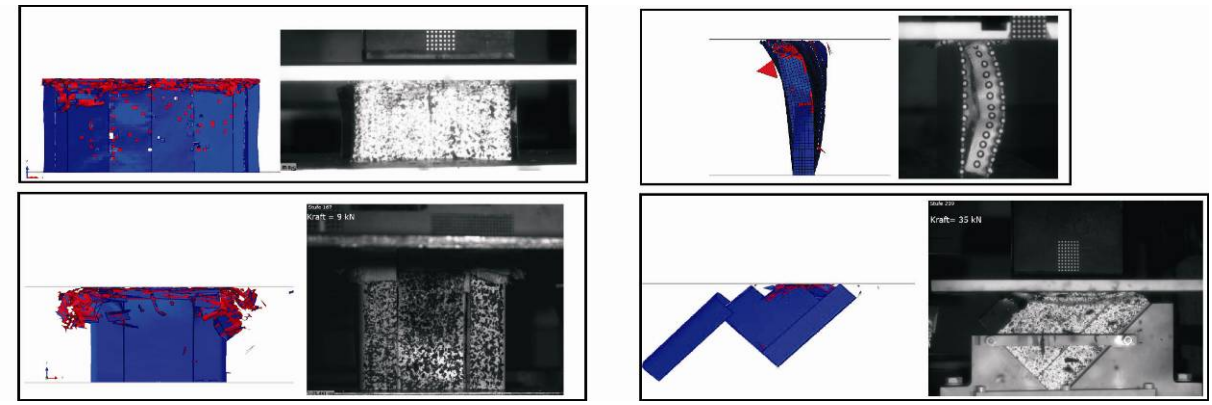


**Figure 7.** Experimental and numerical results of crash loading on structural level: plane and curved spacer structures (top), bonded spacer structures under 0° and 45° loading (bottom)

Structural failure of the front section is dominated by highly localised fibre failure (Figure 8). The numerical calculation was capable to capture this effect as well as the global deformation trend of such large structural assemblies. Additionally, further numerical studies were performed, without an experimental verification to identify the structural behaviour under varying crash load scenarios (45°, 90°).

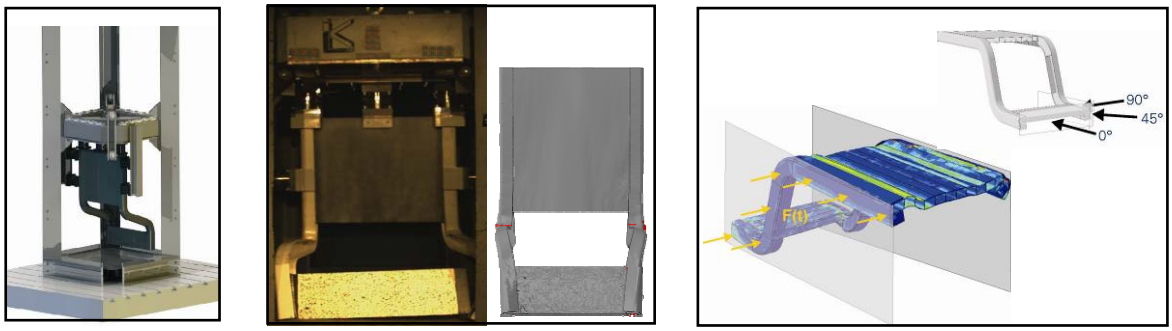


**Figure 8.** Front section crash experiments: drop tower setup (left), experimental and numerical results (middle), additional numerical loading scenarios (right)

## 5 Conclusions

A phenomenological material model for textile reinforced composites was presented, incorporating mode related damage and failure mechanisms and strain rate dependency. It has been implemented in the FE software Abaqus/Explicit using a VUMAT. An experimental methodology was shown, to determine material characteristics. The comprehensive crash and impact experimental work was used for model verification and was therefore continuously accompanied by extensive numerical work. It has been shown, that failure initiation and the corresponding failure modes within the investigated specimens and components are calculated

accurately in terms of their origin and time of occurrence under varying highly dynamic loading cases within the chosen numerical framework. Besides that, the results indicated that further investigations should focus on highly dynamic delamination propagation mechanisms and modelling strategies.

**Acknowledgements**
The authors gratefully acknowledge the financial support of this research by the Deutsche Forschungsgemeinschaft (DFG) within the Collaborative Research Centre (SFB) 639 "Textile-reinforced composites for function-integrating hybrid construction projects in complex lightweight applications", subproject C4.

**References**

[1] Brown K A. Brooks R, Warrior N A. The static and high strain rate behaviour of a commingled E-glass/polypropylene woven fabric composite, *Compos Sci Technol* **7** (2010), pp. 272 - 283

[2] Hufenbach W, Hornig A, Zhou B, Langkamp A, Gude M: Determination of Strain Rate Dependent Through-Thickness Tensile Properties of Textile Reinforced Thermoplastic Composites using L-Shaped Beam Specimens. *Comp. Science and Technology* **71** (2011), pp. 1110-1116

[3] Böhm R, Gude M, Hufenbach W: A phenomenologically based damage model for 2D and 3D-textile composites with non-crimp reinforcement. *Materials and Design* **32** (2011) 5, pp. 2532-2544

[4] Böhm R, Gude M, Hufenbach W: A phenomenologically based damage model for textile composites with crimped reinforcement. *Compos Sci Technol* **70** (2010) pp. 81–7

[5] Cuntze R G: Strength failure conditions of the various structural materials: is there some common basis existing? *SDHM*, **74** (2008), pp. 1–19

[6] Johnson GR, Cook WH: Fracture characteristics of three metals subjected to various strains, strain rates, temperatures and pressures. *Engineering Fracture Mechanics* **21** (1985) 1, pp. 31-48.

[7] Abounaim M, Hoffmann G, Diestel O, Cherif C: Thermoplastic composite from innovative flat knitted 3D multi-layer spacer fabric using hybrid yarn and the study of 2D mechanical properties. *Composites Science and Technology,* **70** (2010), pp. 363-370.

[8] Hufenbach W, Gude M, Ebert C, Zscheyge M, Hornig A: Strain rate dependent low velocity impact response of layerwise 3D-reinforced composite structures. *International Journal of Impact Engineering* **38** (2011), pp. 358–368.

[9] Gude M, Ebert C, Langkamp A, Hufenbach W: *Characterization and simulation of the strain rate dependent material behaviour of novel 3D reinforced Composites.* in Proceedings of the *13th European Conference on Composite Materials (ECCM 13)*, Stockholm, Sweden, (2008).

[10] Hufenbach W, Böhm R, Thieme M, Winkler A, Mäder E, Rausch J, Schade M.: Polypropylene/glass fibre 3D-textile reinforced composites for automotive applications. *Materials and Design* **32** (2011), pp. 1468–1476.

[11] Hufenbach W, Langkamp A, Hornig A, Ebert C.: *Experimental determination of the strain rate dependent out-of-plane properties of textile reinforced composites.* in Proceedings of the *17th International Conference on Composite Materials (ICCM 17)*, Edinburgh, United Kingdom; (2009).

[12] Hufenbach W, Hornig A, Nitschke S, Langkamp A.: *Through-thickness testing and parameter identification of textile reinforced thermoplastic composites for crash and impact calculations*. Proceedings of the *1st International Conference on Composite Dynamics (DYNACOMP)*, Arcachon, France (2012)